Clays and Clay Minerals, Vol. 36, No. 1, 83–93, 1988.

INVESTIGATION OF A K-BENTONITE BY X-RAY POWDER DIFFRACTION AND ANALYTICAL TRANSMISSION ELECTRON MICROSCOPY

W. D. HUFF,[1] J. A. WHITEMAN,[2] AND C. D. CURTIS[3]

[1] Department of Geology, University of Cincinnati
Cincinnati, Ohio 45221

[2] Department of Metallurgy, University of Sheffield
Sheffield S1 3JD, United Kingdom

[3] Department of Geology, University of Sheffield
Sheffield S1 3JD, United Kingdom

Abstract—The <0.1-μm size fraction of an Ordovician K-bentonite from northern Kentucky was characterized by X-ray powder diffraction (XRD). Using A.I.P.E.A. criteria for interstratification nomenclature and Reynolds' computer algorithm the dominant clay mineral proved to be an R2 ordered illite/smectite. The best fit of observed and calculated XRD tracings was obtained using $12 > N > 5$, where N is the number of layers within a diffracting domain.

Sections of the K-bentonite were prepared by ion-beam milling and examined in an analytical transmission electron microscope (ATEM). One-dimensional lattice images observed parallel to the a-b plane showed subparallel packets, about 50–100 Å thick, each of which consisted of about 10-Å thick unit layers. Somewhat thicker unit layers (as much as 14.5 Å) were also seen. The former are presumed to be illite, whereas the latter may be partially collapsed smectite. Selected-area electron diffraction patterns suggested simultaneous diffraction from several packets, each containing at least five layers. Both *h0l* and *0kl* spacings were usually present, indicating that the stacking of the subparallel packets was random. Quantitative analysis by AEM and electron microprobe show the clay to be low in tetrahedral Al but high in octahedral Mg, the latter presumably contributing largely to the interlayer charge responsible for K fixation. The TEM data are broadly reconcilable with the accepted XRD interpretation of a two-component, mixed-layer clay. Alternatively, the TEM images may be interpreted as a single phase having numerous packet boundaries, the latter being responsible for swelling behavior. These two interpretations will not be fully reconciled until greater analytical precision and resolution permit individual packets to be studied. This work suggests that mineral definitions based purely on XRD interpretations may have to be reconsidered as more electron microscope data become available.

Key Words—Analytical transmission electron microscopy, Bentonite, Illite, Interstratification, Potassium, Selected area diffraction, Smectite, X-ray powder diffraction.

INTRODUCTION

The application of high-resolution transmission electron microscopy coupled with energy-dispersive X-ray analysis has greatly enhanced our understanding of illite/smectite interstratification by providing simultaneous chemical, crystallographic, and morphological information on extremely small sample areas. Models of interstratification based upon X-ray powder diffraction (XRD) and elemental analysis have been reexamined (see, e.g., Ahn and Peacor, 1986; Lee *et al.*, 1985; Klimentidis and Mackinnon, 1986; Amouric and Parron, 1985) and reinterpreted (Nadeau *et al.*, 1984a, 1984b; Nadeau and Bain, 1986) in light of these new data. An advantage of analytical transmission electron microscopy (ATEM) is that crystalline aggregates may be examined *in situ* without physical separation or possible disruption of individual crystallites. Elemental and crystallographic data can also be acquired on crystals uncontaminated by non-phyllosilicate minerals (e.g., carbonates). XRD, TEM, ATEM, and electron diffraction data for a K-bentonite are compared here in order to describe the dimensions, orientation, and compositions of the clay crystals.

EXPERIMENTAL

The material investigated was a Middle Ordovician K-bentonite from the High Bridge Group of northern Kentucky. The sample was previously described by Huff and Türkmenoğlu (1981) as sample KB-20 from the Pencil Cave K-bentonite, and comes from a core through the High Bridge Group. It was sufficiently indurated to permit thin section grinding and polishing and subsequent transfer to electron microscope grids for ion-beam milling.

Sample preparation

Specimens prepared for XRD were dispersed in water containing sodium hexametaphosphate by placing the beaker in an ultrasonic bath for 20 min and then allowing it to stand long enough for the <2-μm size

fraction to settle. The <0.1-μm fraction was separated from the remaining suspension by centrifugation and sedimented onto glass petrographic slides. The slides were placed in a desiccator jar containing ethylene glycol and heated at 50°C for 12 hr. The jar was then removed from the oven and the slides kept in it at room temperature for an additional 4 days to permit complete saturation by the vapor. XRD scans were made on a Philips diffractometer using CuKα radiation at a scan rate of 0.25°2θ/min. XRD tracings were modeled using the MOD10S program of R. C. Reynolds (Dartmouth College, Hanover, New Hampshire, personal communication, 1982).

TEM specimens were prepared from thin sections of the core sample. Chips were hand cut, dry ground, and attached to the petrographic slide with Lakeside cement. After further dry grinding to minimum possible thickness the slide was reheated on a hot plate, the section was cut into a number of 3-mm-diameter circles with a scalpel, and each circle was attached to a copper TEM grid with epoxy resin. After cleaning the residual Lakeside with solvent the samples were thinned further by ion-beam milling. Samples were examined in a Philips 400T transmission electron microscope equipped with an energy-dispersion X-ray analyzer and operated at 100 kV. The same material was also analyzed by a Cambridge Microscan 9 electron microprobe using a 2-μm-diameter spot size. Data from both analytical techniques were cast into structural formulae assuming 12 oxygens per unit cell. ATEM data were developed from measurements of element ratios, because absolute intensities relative to standards could not be obtained (as is possible in electron microprobe analysis). Oxide analyses were thus derived only by assuming stoichiometric oxygen and normalizing to 100%. Comparison with electron microprobe analyses demanded that the data be treated similarly. The alternative, to assume some value for structural water for the ATEM data, was less valid.

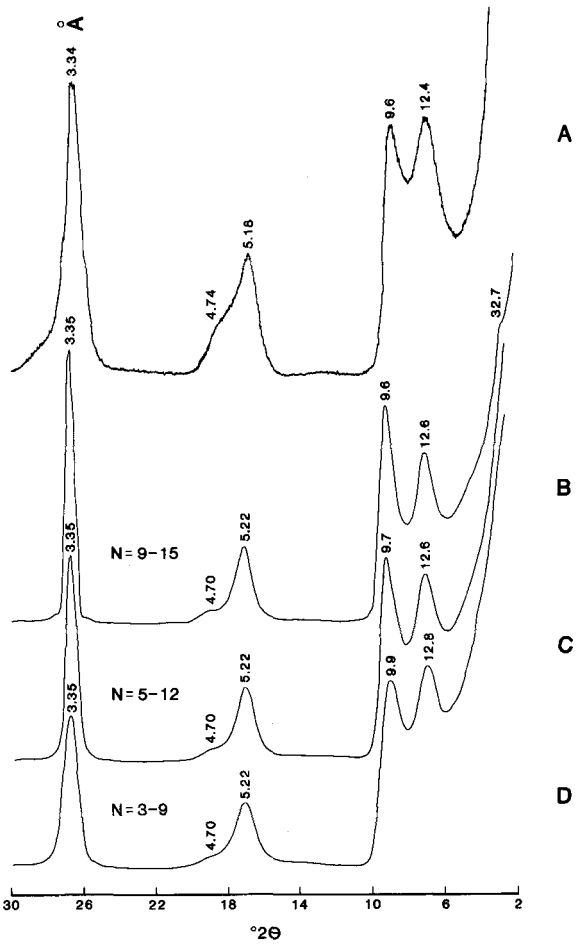

Figure 1. X-ray powder diffraction (XRD) tracings of sample KB-20 run with CuKα radiation. Patterns represent oriented samples of <0.1-μm material saturated with ethylene glycol. (A) Observed diffraction tracing. Peak positions and intensities indicate ISI ordering. (B)–(D) Computer-generated XRD patterns of ordered I/S having 80% I. Other parameters used are Σ = 12, Si = 3.75, Fe = 0.14, K = 0.65. Probability factors are C = .800, XC = .999, XCC = .750, and XCCC = .650. Values for N represent thickness of diffracting domains.

RESULTS AND DISCUSSION

X-ray powder diffraction

XRD tracings of the ethylene glycol-saturated, <0.1-μm clay fraction of sample KB-20 are typified by Figure 1A, which shows the low-angle double peak characteristic of ordered illite/smectite (I/S). The absence of a superlattice reflection between 2° and 3°2θ suggests that the ordering is long-range or ISI-type (Reynolds, 1980) and that it closely resembles the theoretical Reichweite R2 ordering (Inoue and Utada, 1983). Środoń *et al.* (1986) referred to similar patterns as R1/R3 ordered. Computer-simulated patterns were generated that closely approximated, but did not precisely reproduce, the XRD tracing. Figures 1B–1D illustrate three calculated patterns consisting of 80% collapsed illite and 20% expanded smectite layers, using the MOD10S program of Reynolds (1982). The peak at about 17°2θ is considered more reliable for estimating component percentages than are the low-angle peaks, due to a difference in sensitivity to a number of variables, including particle size and thickness, degree of preferred orientation, the Lorentz factor, and the presence of illite-smectite segregation (Reynolds, 1980). Środoń (1980) also showed that the assumed thickness of the ethylene glycol-smectite layer can vary. The three calculated tracings in Figure 1 are based on the probability of two collapsed layers following an expanded layer (XCC in the program) equal to .750 and the probability of three collapsed layers following an expanded layer (XCCC) equal to .650. The near fit suggests indeed that some segregation of illite and smectite layers existed in the sample. Nadeau *et al.* (1984a, 1984b) showed that similar clays are composed of thin illite

https://doi.org/10.1346/CCMN.1988.0360111 Published online by Cambridge University Press

particles, 2–16 silicate layers thick, whose interfaces are capable of combining with water and organic molecules to produce smectite-like interlayers and interparticle diffraction effects resulting in XRD data similar to those of interstratified I/S clays.

Variations in the low-angle peak positions, widths, and intensities of peaks occurred with changes in the value of N, the range of thicknesses of unit layers making up the diffracting domain in the interference function. With all other variables held constant, the computed pattern for very thick domains (N = 9–15) produced relatively narrow peaks with shifts in the high 2θ direction and a low-angle reflection at 32.7 Å. N values of 5–12 and 3–9, produced broader peaks with different relative intensities and shifts in the low 2θ direction. Higher angle peaks near 17° and 27°2θ were not affected. The best fit pattern was for N = 5–12 (Figure 1C), which suggests a minimum size for diffracting crystals. Actual three-dimensional crystals may have been thicker than this and may have been made up of many domains, but without assuming interparticle diffraction the minimum thickness range was 5–12 illite units or 50–120 Å.

Transmission electron microscopy

One-dimensional, bright-field lattice images of sample KB-20 revealed an *in situ* fabric of thin, flexible, subparallel units having a high degree of preferred orientation. Effective image contrast required that (00*l*) be oriented parallel to the incident electron beam, together with a proper defocussing of the optical system. Under ideal conditions individual structural units in phyllosilicates could be resolved to show stacking disorders, interstratification, and other details described in previous XRD studies (e.g., Klimentidis and Mackinnon, 1986; Ahn and Peacor, 1986). Distortion in either the vertical or horizontal plane of the bombarded sample resulted in discontinuous imaging, and the sample appeared to contain localized aggregates of crystalline material; in some instances, the pattern was entirely featureless. Figure 2 shows both of these characteristics in K-bentonite. Imaged packets of units ranging from 2 to 20 silicate layers in thickness pass in and out of the focal plane of the microscope. Dark patches indicate undulatory distortion in the packets and commonly extend across subparallel grain boundaries to adjacent crystallites. Non-imaged portions of the samples are considered to be segments of crystals twisted or warped sufficiently to take them out of parallel alignment with the electron beam. Damage from the electron beam undoubtedly contributed to the loss of image as well, considering the fragility of hydrous layer silicates under high vacuum and the difficulty of obtaining any image contrast stable enough to photograph. Although almost continuous imaging of crystals was possible over distances of more than 1000 Å (Figure 2), large regions existed in which imaging did not occur. Amouric and Parron (1985) interpreted such regions as consisting of the decompositions product of a hypothetical "phase X," which presumably converts into noncrystalline matter before converting further into well-crystallized phyllosilicate. Our data do not support this interpretation inasmuch as portions of the same crystallites were seen to pass in and out of focus. Most probably, these areas were simply distorted with respect to the beam orientation.

Figures 2b and 2c are enlargements of Figure 2a and show the typical features of edge dislocation and crystallite subparallelism reported by other authors (e.g., Lee *et al.,* 1985; Ahn and Peacor, 1985, 1986). Domains as thick as 500 Å can be seen to be composed of smaller units averaging about 10 unit layers in thickness, which seem to split off separately at the ends of crystals or merge separately with adjacent crystallites along low-angle boundaries. Thus, large domains appeared to be composites of smaller units, which nevertheless retained some internal coherence of their own. Small dislocations within the larger crystal may represent compositional anomalies or perhaps imperfections in the stacking sequence of individual layers similar to interfaces between the coherent domains.

Spacings between layers were about 10 Å, but the uncertainty of the behavior of expandable clays under high vacuum (Ahn and Peacor, 1986) made it impossible to distinguish precisely between smectite and illite. Furthermore, boundaries between the units may have made up the smectite-like interlayers, as suggested by Vali and Köster (1986). In any case, untreated smectite interlayers may have collapsed to spacings equal to or near the 10-Å spacing of illite, and thus under high magnification these minerals might have both given similar spacings. Vali and Köster (1986) compared K-bentonite I/S expanded with octadecylammonium ions and untreated I/S and showed what appeared to be smectite layers having 17-Å spacings. Their data, however, did not clearly distinguish illite from smectite in terms of concepts of interstratification based on XRD. Both electron diffraction data and microdensitometer scans of sample KB-20 lattice images indicated spacings between 10 and 14.5 Å within the same domain packet. Layer spacings in the large domain in Figure 4 averaged 10.3 Å and varied unsystematically from slightly less than 10 Å to 13.4 Å, presumably representing both collapsed and partially expanded layers.

Similar spacings were noted for units shown in Figure 3. In Figure 3a a packet of five-unit interlayers averages 14.5 Å per layer, suggesting that some smectite existed as a segregated phase from illite. It is unclear from TEM data whether these layers pass laterally into illite or are consistently smectite-like internally and are interlayered with illite packets. Similar features were reported by Ahn and Peacor (1986) for samples from

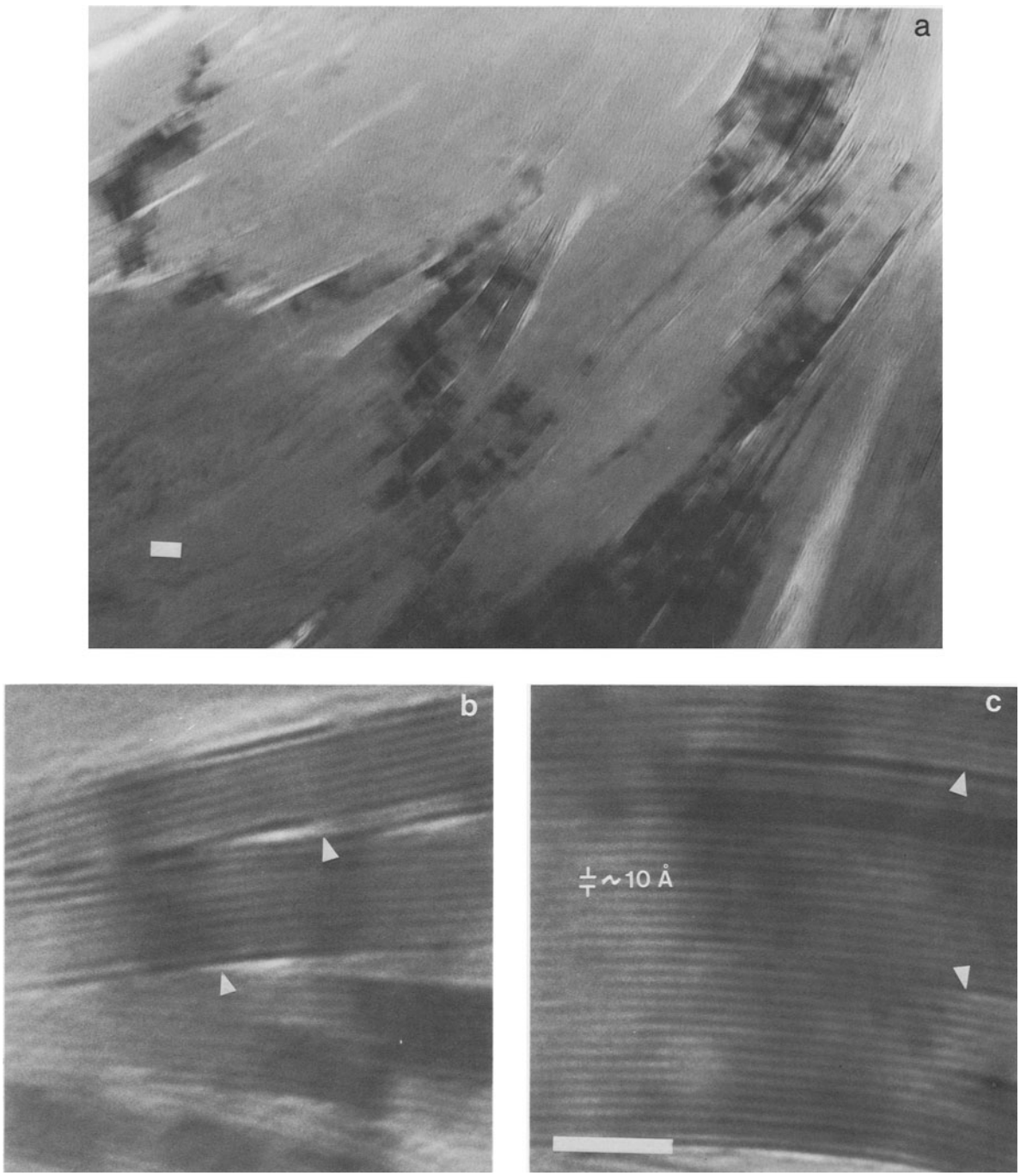

Figure 2. Bright-field lattice images of sample KB-20. (a) Subparallel packets of crystallites contain 3–20 layers. Non-imaged areas are due to beam damage and/or non-focusing of the beam. Imaged areas show predominance of thin, flexible packets consisting of 10-Å units. (b) Edge dislocations at grain boundaries arise from subparallel growth of the crystallites. (c) Several small dislocations between layers may represent either partially collapsed smectite or compositional inhomogeneities. Scale bar equals 100 Å.

Gulf Coast shale and were interpreted by them as representing an intermediate stage in the transformation of smectite to illite. Whereas Ahn and Peacor (1986) found illite and smectite as discrete monomineralic packets, we found both collapsed and partially expanded units to be intimately associated. Precise determination of stacking geometry was precluded because of the difficulty in measuring the expanded

https://doi.org/10.1346/CCMN.1988.0360111 Published online by Cambridge University Press

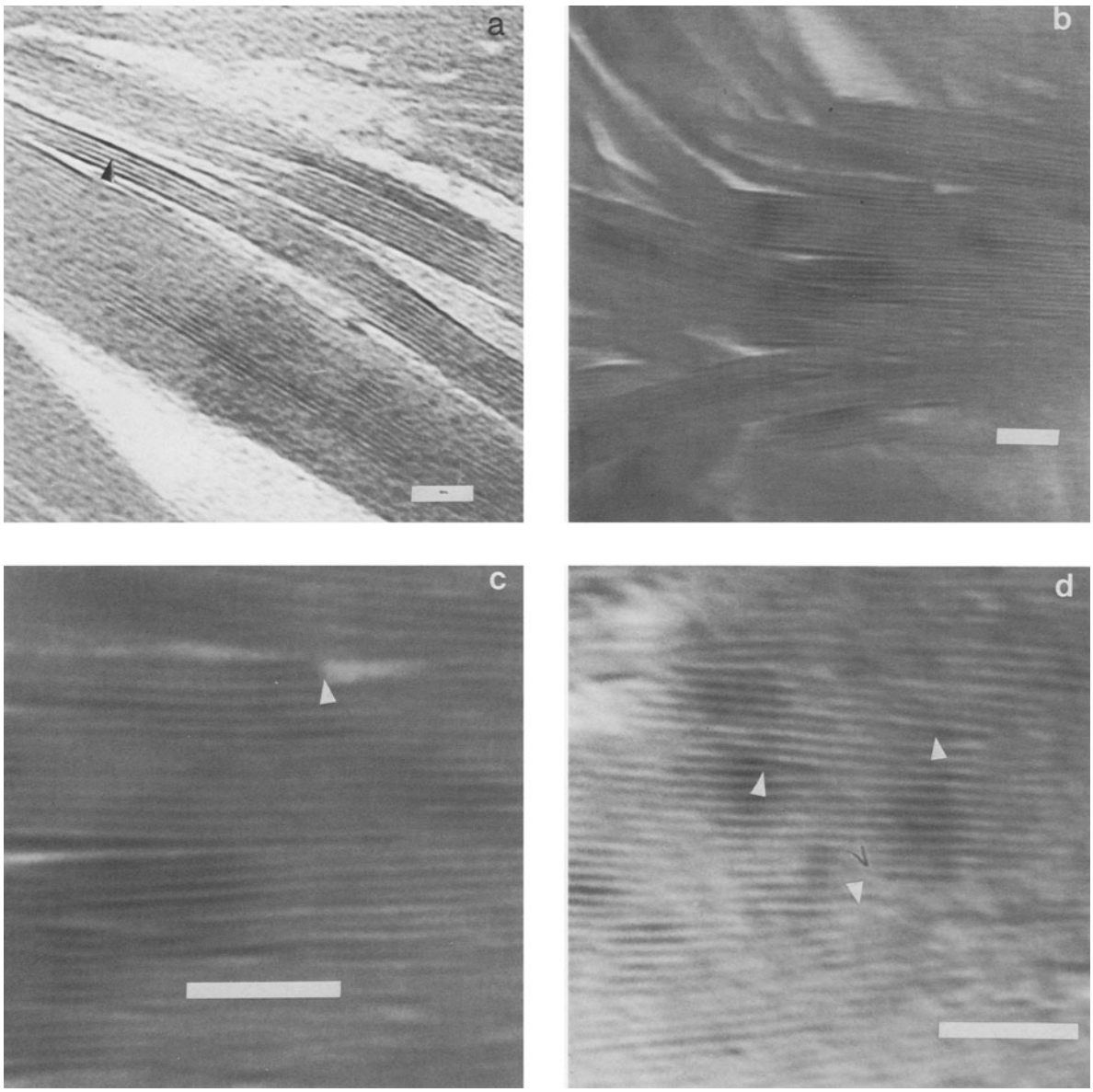

Figure 3. Bright-field lattice images showing (a) some layers with spacings greater than 10 Å that may represent incompletely collapsed smectite. (b) Some small crystallites contain relatively few defect structures. (c) Note uniform 10-Å spacing of individual layers within packets averaging 5–10 units thick; and (d) dislocations along some 10-Å layers and at boundaries with adjacent crystallites. Scale bar equals 100 Å.

spacings. In general, lattice images of K-bentonite did not resemble I/S formed by relatively rapid burial metamorphism. If smectite was present in the K-bentonite, it was as uniform and as well-ordered in appearance as the illite and did not exhibit the wavy and irregular habit of, for example, Gulf Coast smectite. Crystallites of discrete smectite and illite and I/S had about the same dimensions in crystallite packets and the same uniformity of parallelism among adjacent layers, thereby precluding unequivocal identification of each phase, although detailed measurements of unit spacings and chemical and XRD data suggest that both smectite and illite were present.

Selected area diffraction

SAD patterns were made with a 1-μm aperture of areas adjacent to those shown in lattice images. The rapid deterioration of the clay in the presence of an electron beam operating at 100 kV precluded both imaging and SAD analysis of the same spot, but the general continuity of crystal morphology and fabric over distances of several micrometers provided reasonable

https://doi.org/10.1346/CCMN.1988.0360111 Published online by Cambridge University Press

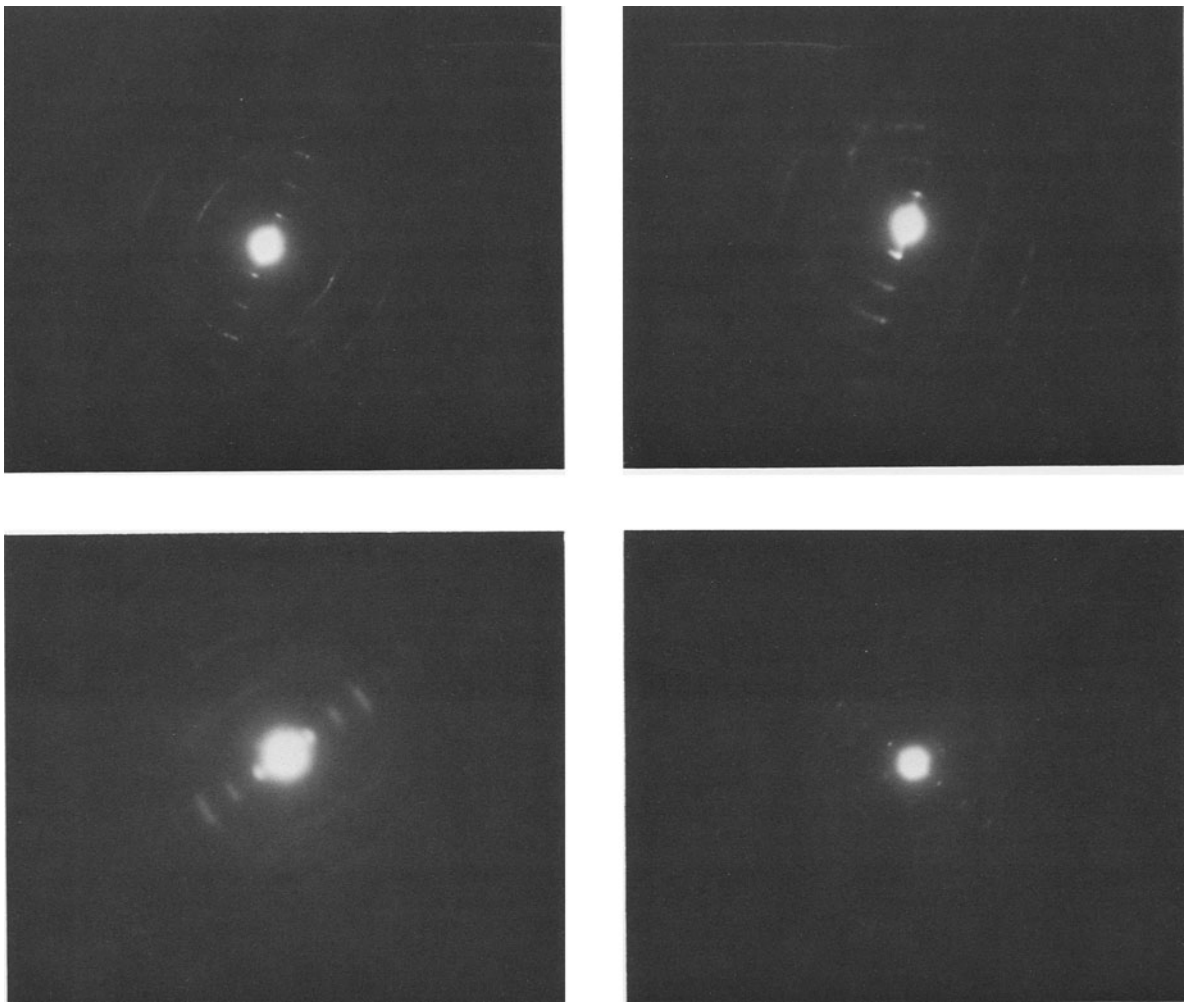

Figure 4. (Upper) Selected area diffraction (SAD) patterns of K-bentonite crystallite packet showing uniform 10-Å spacing of 001 along c* and blurred 0*kl* lines. (Lower) Several packets in subparallel arrangement with insufficient thickness to produce nearly complete circles, indicating very limited thickness of diffraction crystallite, probably 3–5 illite units thick. 001 reflections from two individual crystallites can be seen.

confidence that the SAD patterns and images were of the same material.

Typical SAD patterns of K-bentonite consisted of a rather well-defined row of 00*l* spots (Figure 4). Consistency in intensity and spacing suggest the polytype was 1*M*. The spots commonly occurred as linear blurs normal to 00*l*, which, when resolved, were closely spaced spots from several subparallel units. Additional *hkl* spots were either weak or absent and where present had blurred into semicircles and discontinuous rings. Spacings along 00*l* (c*) varied from 9.9 Å to 10.3 Å and were generally more characteristic of illite than smectite (see Lee *et al.*, 1984; Ahn and Peacor, 1986) in that as many as six orders were easily resolved. The mean of 10 measurements of d(001) on a calibrated slate gave 001 = 10.00 Å and σ = 0.13; these values are within experimental error. Resolution of 00*l* reflections indicated that diffraction was occurring along crystallographic planes oriented parallel to the electron beam. Each diffracting domain consisted of some multiple number of parallel layers with d(001) $\simeq$ 10 Å in the direction of c*. Figure 5 illustrates the relationships between crystal thickness and the consequent SAD pattern of the reciprocal lattice. For crystals one unit cell in thickness, diffraction by an incident beam parallel to the ab plane will produce solid lines representing *hkl* planes. For some small but finite number of layers (N $\approx$ 3) the lines began to resolve into dashed lines with the distance between the dashes proportional to the number of diffracting layers. For still thicker (N $\approx$ 10) crystal having all layers stacked in crystallographic continuity, *hkl* spots were clearly observed. Thus, from this standpoint K-bentonites appear to be composed of small crystallites more than 2 or 3 unit cells thick,

https://doi.org/10.1346/CCMN.1988.0360111 Published online by Cambridge University Press

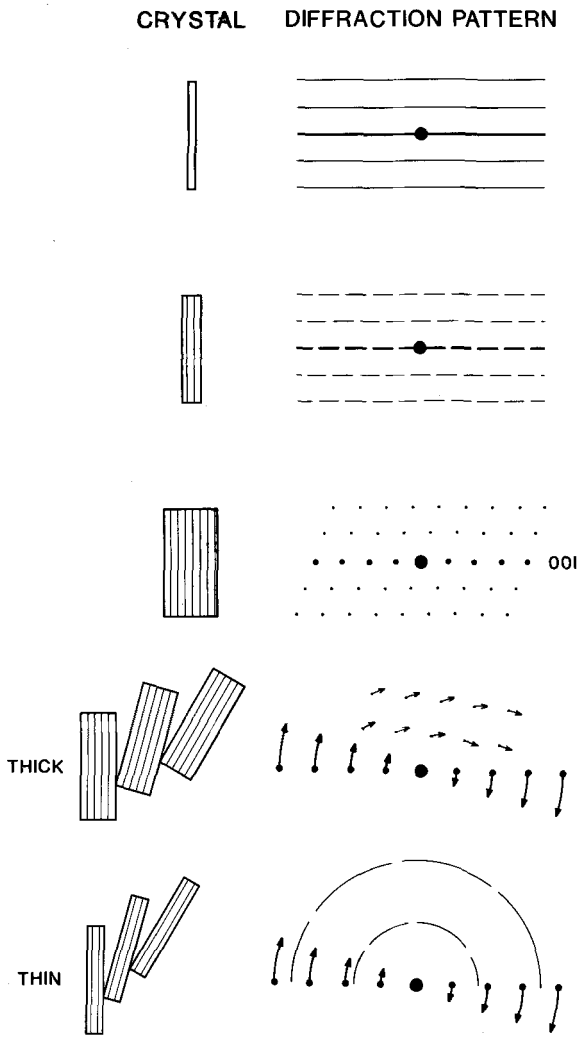

Figure 5. (Top) Relationship between crystallite orientation and thickness and consequent selected-area diffraction pattern. (Bottom) Relationship between thickness and orientation of crystallite packets and resultant 0*kl* reflections. See text for discussion.

but generally not more than 12 unit cells thick and not as well crystallized as micas.

Figure 4 shows three examples of blurring of *hkl* spots that are typical of packets of crystallites each situated parallel to the incident beam, but stacked subparallel to one another. The fanning of 00*l* spots normal to c* was the result of simultaneous diffraction from small, multilayer crystallites arranged in a pattern of low-angle divergence (Figure 5B). The thicker the individual crystallites, the more other *hkl* lines were resolved as spots. For very thin crystallites, the spots merged into discontinuous rings. Both features are illustrated in Figure 4 which shows discernible 0*kl* and *h*0*l* reflections merging into discontinuous concentric rings. An extreme example (i.e., very small crystals) is shown in Figure 4C; here the rings are nearly complete circles of fairly uniform density. These observations support the interpretation of lattice images in which the crystallites are 5–10 unit cells thick.

Figure 5 shows two sets of superimposed reflections having d-values of about 4.4 and 2.6 Å. Rotation of a single illite (mica) crystal about an axis perpendicular to 00*l* will create strong diffracting conditions every 30° corresponding to the pseudohexagonal prism directions of the crystal. Consideration of the geometry of the tetrahedral sheet shows the existence of essentially two strong sets of atom alignment and thus two strong sets of diffracting planes. These sets coincide with the *a* and *b* crystallographic axes and those directions related to them by symmetry. A single crystal rotated 30° about an axis perpendicular to 00*l* will produce reciprocal lattice *hkl* reflections alternately at one of two distances from 00*l*. These distances correspond to a* and b*. Thus, diffraction patterns produced in any of the symmetry positions which give rise to diffraction effects may be indexed by determining the distance from 00*l*. The angle β^* between this and c* will vary between 90° and 96° for crystals with monoclinic symmetry.

Figure 6 shows these two geometries for mica from a Welsh slate. The two orientations are 90° from each other and would be repeated in rotational increments of 60°, the only apparent difference being in the precise value of β^*. Consequently, different structural interpretations of electron diffraction data can result from purely geometric effects.

We have shown that the superimposed reflection sets resulted from units stacked randomly in the c-axis direction. The random stacking faults may correspond to the interfaces separating coherent illite units. Those units that happened to be oriented with a* or b* orthogonal to the electron beam will have produced either of these two mica-zone-axis diffraction patterns. If this phenomenon is coupled with the very thin nature of the crystallites and their subparallel orientation, all features of the diffraction patterns can be easily explained. Little evidence was found for a clear two-phase mixture, such as that reported by Lee *et al.* (1984) for chlorite and illite, possibly because most of the smectite had collapsed to spacings only 0.3 Å greater than that of the illite. The larger units yielded diffraction features which are indicative of illite layers. Thus, little evidence was found for ordered interstratification of illite and smectite layers within the larger units.

Chemistry

Chemical analyses from both analytical electron microscopy and electron microprobe showed a general agreement between the normalized values for major elements (Table 1). Rapid deterioration of I/S in the presence of the electron beam made it difficult to image

https://doi.org/10.1346/CCMN.1988.0360111 Published online by Cambridge University Press

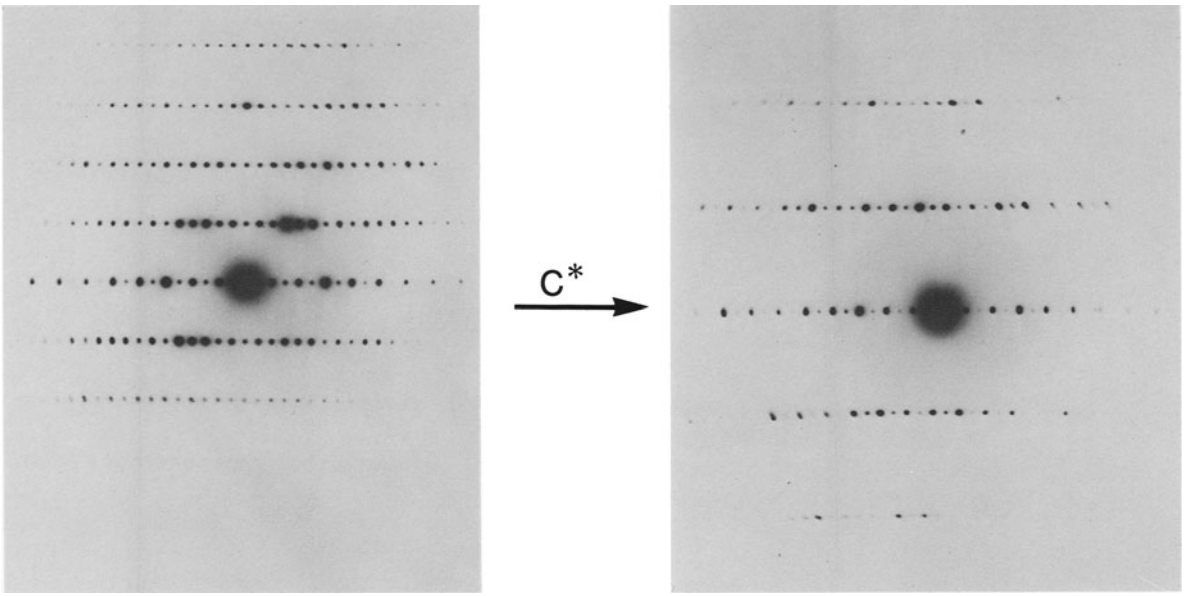

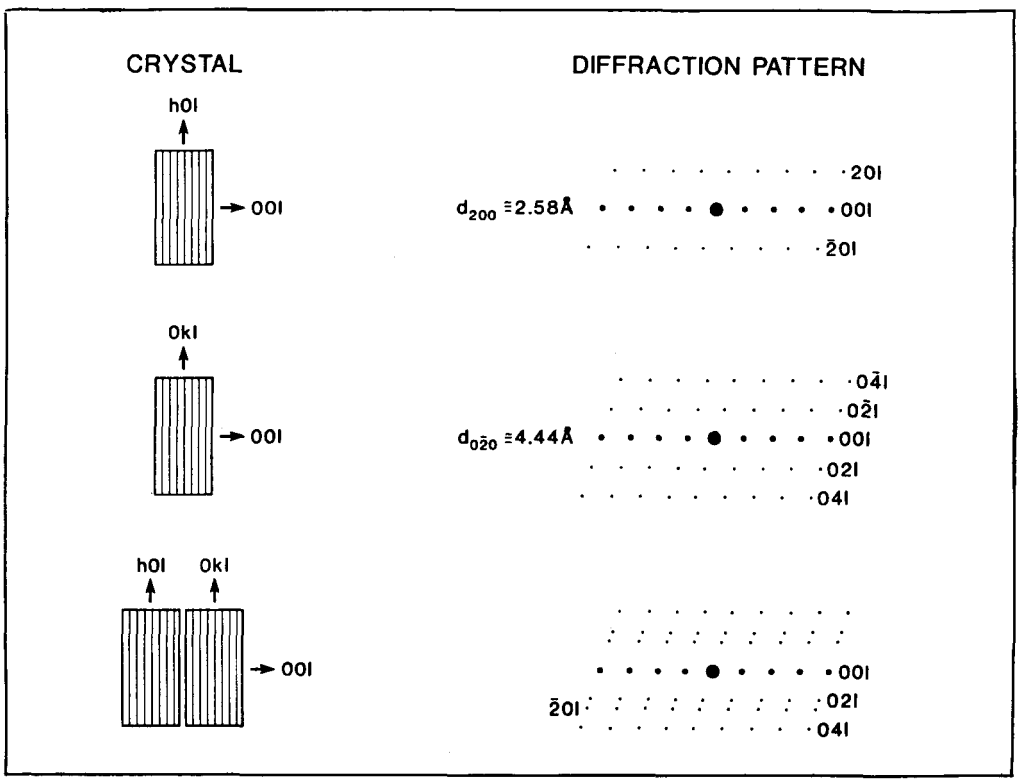

Figure 6. (Upper) X-ray diffraction (SAD) patterns of well-crystallized mica from a Welsh slate showing differences in width of rows as a function of crystal orientation. Crystal has been rotated 30° about an axis parallel to c* producing first 0*kl*, and then *h*0*l* reflections. (Lower) Diagrammatic explanation of relationship shown above. SAD patterns taken 30° apart record a* and b* dimensions. Random stacking of packets produces a superimposed pattern of both crystallographic orientations.

and analyze the same spot by ATEM, but the clustering of clay packets in K-bentonite permitted different portions of packets more than 500 Å wide to be examined in several spots. Reproducibility was generally good for all elements, although probe and ATEM values for some elements were not in complete agreement. Mg and Fe were higher in the probe analyses and K and Na were lower, compared with those by ATEM. Vari-

https://doi.org/10.1346/CCMN.1988.0360111 Published online by Cambridge University Press

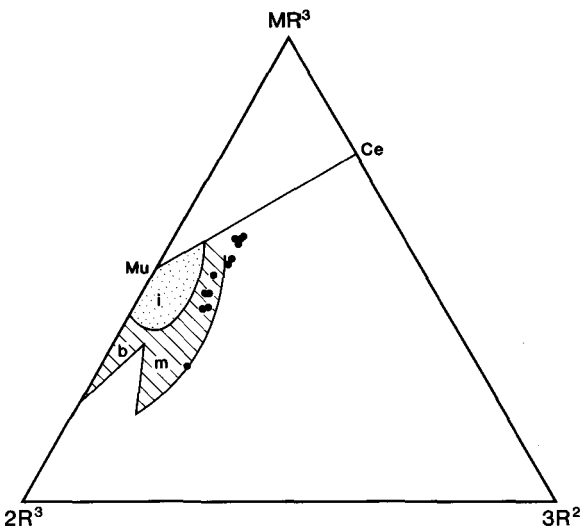

Figure 7. Plot of analytical transmission electron microscopy data on Velde diagram. MR^3 is influenced mainly by K, Ca, and Na; $2R^3$ by Al plus Fe; and $3R^2$ by Mg. Plots fall generally in the region characterized by mixed-layer illite/montmorillonite clays below the muscovite-celadonite join. Regions identified are i = illite, b = beidellite, and m = montmorillonite. Effect of octahedral Mg is to move the points away from the illite-muscovite field.

ations in K values may have been caused by volatilization and diffusion (Lee *et al.*, 1984) during count times, and Na may have similarly been affected. Mg and Fe differences may possibly reflect differences in technique, however, both elements varied within each technique as well as between them. Thus, some evidence exists of real compositional inhomogeneity within K-bentonite packets.

If the data are cast into structural formulae and compared with published analyses of I/S (Środoń *et al.*, 1986; Hower *et al.*, 1976; Hower and Mowatt, 1966), tetrahedral Al is generally lower and octahedral Mg higher than samples with equivalent I/S ratio based on XRD. If all the Mg is located in the octahedral sheet and is not an exchangeable cation, the total layer charge is −0.70, which agrees well with the data of Środoń *et al.* (1986) for Silurian and Carboniferous K-bentonites, but which is slightly higher than that for Cretaceous K-bentonites from Montana. Hower *et al.* (1976) proposed a model for the illitization of smectite which accounted for an increase in the total layer charge as a result of Al-for-Si substitution in the tetrahedral sheet. Octahedral substitution contributes little to the overall layer charge in this model and, in fact, Mg and Fe are thought to be released during the illitization process. Calculation of the half-cell structural formula for Ordovician K-bentonite I/S suggests octahedral Mg may, under certain circumstances, play an important role in controlling layer charge. Ahn and Peacor (1986) concluded from their study of Gulf Coast illitization that

Table 1. Average[1] analytical transmission electron microscopy (ATEM) and electron microprobe analyses for K-bentonite.

Oxide	ATEM	Microprobe
SiO_2	60.72[2]	61.64[3]
Al_2O_3	22.09	23.03
Fe_2O_3	2.54	1.78
MgO	5.73	4.77
CaO	0.31	0.30
Na_2O	0.37	0.67
K_2O	7.76	8.23
Total	99.52	100.00

ATEM half-cell formula $(Si_{3.75}Al_{0.25})(Al_{1.35}Fe^{3+}_{0.12}Mg_{0.53})$-$(Ca_{0.01}Na_{0.04}K_{0.61})O_{10}(OH)_2$.[4]

Microprobe half-cell formula $(Si_{3.77}Al_{0.23})(Al_{1.44}Fe^{3+}_{0.08}$-$Mg_{0.44})(Ca_{0.02}Na_{0.08}K_{0.64})O_{10}(OH)_2$.

[1] Average of 11 spots for ATEM and 4 spots for microprobe.

[2] Normalized to 6 oxygens. Omission of Ti, not considered to be structurally held, accounts for total less than 100%.

[3] Normalized to 100%.

[4] Calculation assumes smectite component is dioctahedral.

apparent contradictions between XRD and ATEM data can be resolved only by assuming rather severe disruption of tetrahedral-octahedral bonds during transformation. Illite thus forms first as isolated packets within preexisting smectite by means of both K-fixation and tetrahedral/octahedral substitution. The high Mg content of Ordovician K-bentonite requires either substantial Mg-substitution during illitization or the existence of a high-Mg precursor smectite. Most studies of illitization reactions, however, indicated a reduction of octahedral Mg (Inoue and Utada, 1983; Eberl, 1978; Nadeau and Bain, 1986) and a net increase in octahedral charge (Eslinger *et al.*, 1979). Thus, K-bentonite having high octahedral Mg probably retained this charge from the parent smectite.

A comparison of the I/S composition of K-bentonite determined by ATEM with those of illite and smectite is shown in Figure 7, plotted after the method of Velde (1985). Data points generally fall in the field representing natural mixed-layer illite/montmorillonite. Inconsistencies in the amount of measured K may explain some of the scatter, such as the single point near the 2R corner, but the general agreement with microprobe data suggests that the variation is real. Ahn and Peacor (1986) described compositional variation of a similar nature in Gulf Coast I/S. Thus, a high-Mg smectite may have been the precursor of the neoformed I/S, and a principal cause of the total layer charge can be attributed to octahedral site occupancy by Mg. This model is supported by the conclusions of Lahann and Roberson (1980) that Si dissolution from smectite and consequent substitution by Al is retarded in high-Mg varieties. Alternatively, of course, the availability of abundant Mg during diagenesis may have given rise to Mg-rich clay crystals.

SUMMARY AND CONCLUSIONS

Application of a multiple analytical approach of XRD, HRTEM, ATEM, SAD, and electron microprobe permitted a reconsideration and reinterpretation of earlier models of I/S structure which were based upon XRD of dispersed particles and bulk chemical analysis. The interpretation of ATEM data has already been extensively treated in the literature and has shown that care must be taken to avoid misinterpretation of basal spacings, interlayer distances, structural defects, and order/disorder phenomena in layer stacking arrangements (Klimentidis and Mackinnon, 1986; Lee *et al.,* 1984; Ahn and Peacor, 1986; Ijima and Buseck, 1978). One-dimensional lattice images of untreated I/S cannot be interpreted unambiguously without further information on composition and fabric of crystallites and without careful attention to the phase-contrast mechanism that gives rise to fringes. Partial or complete collapse of smectite layers may occur either during ion thinning or in the microscope sample chamber. Treatment with organic expansion reagents may sustain some smectite in expanded form, but does not necessarily ensure a clear distinction between the illite and smectite phases (Lee and Peacor, 1986).

Although the exact relationship of the lattice-fringe image contrast to the atomic structure is not known with certainty, SAD patterns confirm the presence of small, crystallites having first-order basal spacings both equal to and greater than 10 Å. These crystallites are randomly stacked in the c-axis direction as shown by streaking of combined *h*0*l* and 0*kl* reflections. Ahn and Peacor (1986) reported that most of the illite and smectite in Gulf Coast shale exists as discrete packets of each and that their physical appearance on lattice images permits visual identification of both.

We have found evidence of I-S segregation in XRD patterns, and both TEM and SAD data indicate the abundance of small (50–100 Å thick) crystallites. Our data do not, however, indicate a similarity between I/S in K-bentonites and Gulf Coast shale.

Data provided by ATEM is in general agreement with the accepted model for I/S of a two-component, interstratified clay based on XRD; however, this interpretation does not preclude the possibility of I/S consisting of a single phase with numerous packet boundaries which provide the swelling behavior generally attributed to smectite. Individual packets and their external surfaces must be examined with greater precision and resolution before these two interpretations can be fully reconciled.

ACKNOWLEDGMENTS

This research was undertaken while W. D. Huff was on academic leave from the University of Cincinnati. He acknowledges the support of NSF grant INT-8419409 and the use of research facilities at the University of Sheffield, under the direction of J. B. Dawson, department head. The manuscript was improved through comments by reviewers P. H. Nadeau and D. R. Peacor and editor F. A. Mumpton.

REFERENCES

Ahn, J. H. and Peacor, D. R. (1985) Transmission electron microscope study of diagenetic chlorite in Gulf Coast argillaceous sediments: *Clays & Clay Minerals* **33,** 228–236.

Ahn, J. H. and Peacor, D. R. (1986) Transmission and analytical electron microscopy of the smectite-to-illite transition: *Clays & Clay Minerals* **34,** 165–179.

Amouric, M. and Parron, C. (1985) Structure and growth mechanism of glauconite as seen by high-resolution transmission electron microscopy: *Clays & Clay Minerals* **33,** 473–481.

Eberl, D. (1978) Reaction series for dioctahedral smectites: *Clays & Clay Minerals* **16,** 327–340.

Eslinger, E., Highsmith, P., Albers, D., and DeMayo, B. (1979) Role of iron reduction in the conversion of smectite to illite in bentonites in the Disturbed Belt, Montana: *Clays & Clay Minerals* **27,** 327–338.

Hower, J., Eslinger, E. V., Hower, M. E., and Perry, E. A. (1976) Mechanism of burial metamorphism of argillaceous sediment: 1. Mineralogical and chemical evidence: *Geol. Soc. Amer. Bull.* **87,** 725–737.

Hower, J. and Mowatt, T. C. (1966) The mineralogy of illites and mixed-layer illite-montmorillonite: *Amer. Mineral.* **51,** 825–854.

Huff, W. D. and Türkmenoğlu, A. G. (1981) Chemical characteristics and origin of Ordovician K-bentonites along the Cincinnati arch: *Clays & Clay Minerals* **29,** 113–123.

Iijima, S. and Buseck, P. R. (1978) Experimental study of disordered mica structures by high-resolution electron microscopy: *Acta Crystallogr.* **A34,** 709–719.

Inoue, A. and Utada, M. (1983) Further investigations of a conversion series of dioctahedral mica/smectites in the Shinzan hydrothermal alteration area, northeast Japan: *Clays & Clay Minerals* **31,** 401–412.

Klimentidis, R. E. and Mackinnon, I. D. R. (1986) High-resolution imaging of ordered mixed-layer clays: *Clays & Clay Minerals* **34,** 155–164.

Lahann, R. W. and Roberson, H. E. (1980) Dissolution of silica from montmorillonite, effect of solution chemistry: *Geochim. Cosmochim. Acta* **44,** 1937–1943.

Lee, J. H., Ahn, J. H., and Peacor, D. R. (1985) Textures in layered silicates: Progressive changes through diagenesis and low-temperature metamorphism: *J. Sed. Petrol.* **55,** 532–540.

Lee, J. H. and Peacor, D. R. (1986) Expansion of smectite by laurylamine hydrochloride: Ambiguities in transmission electron microscope observations: *Clays & Clay Minerals* **34,** 69–73.

Lee, J. H., Peacor, D. R., Lewis, D. D., and Wintsch, R. P. (1984) Chlorite-illite/muscovite interlayered and interstratified crystals: A TEM/STEM study: *Contrib. Mineral. Petrol.* **88,** 372–385.

Nadeau, P. H. and Bain, D. C. (1986) Composition of some smectites and diagenetic illitic clays and implications for their origin: *Clays & Clay Minerals* **34,** 455–464.

Nadeau, P. H., Tait, J. M., McHardy, W. J., and Wilson, M. J. (1984a) Interstratified XRD characteristics of physical mixtures of elementary clay particles: *Clay Mineral.* **19,** 67–76.

Nadeau, P. H., Wilson, M. J., McHardy, W. J., and Tait, J. M. (1984b) Interstratified clays as fundamental particles: *Science* **225,** 923–925.

Reynolds, R. C. (1980) Interstratified clay minerals: in *Crystal Structures of Clay Minerals and their X-ray Identification,* G. W. Brindley and G. Brown, eds., Mineralogical Society, London, 249–303.

Środoń, J. (1980) Precise identification of illite/smectite interstratification by X-ray powder diffraction: *Clays & Clay Minerals* **28,** 401–411.

Środoń, J., Morgan, D. J., Eslinger, E. V., Eberl, D. D., and Karlinger, M. R. (1986) Chemistry of illite/smectite and end-member illite: *Clays & Clay Minerals* **34,** 368–378.

Vali, H. and Koster, H. M. (1986) Expanding behaviour, structural disorder, regular and random irregular interstratification of 2:1 layer-silicates studied by high-resolution images of transmission electron-microscopy: *Clay Mineral.* **21,** 827–859.

Velde, B. (1985) *Clay Minerals: A Physio-Chemical Explanation of their Occurrence:* Elsevier, New York, 427 pp.

(Received 16 March 1987; accepted 3 October 1987; Ms. 1656)